Interfacial Behavior of Perchlorate versus Chloride Ions in Aqueous Solutions

Marcel D. Baer,[†] I-Feng William Kuo,*[,‡] Hendrik Bluhm,[§] and Sutapa Ghosal*[,‡,∥]

Lehrstuhl für Theoretische Chemie, Ruhr-Universität Bochum, D-44780 Bochum, Germany, Physical and Life Sciences Directorate, Lawrence Livermore National Laboratory, L-437, Livermore California 94551, and Chemical Sciences Division, Lawrence Berkeley National Laboratory, Berkeley, California 94720

Received: June 5, 2009; Revised Manuscript Received: October 19, 2009

In recent years, theoretical as well as experimental studies have presented a novel view of the aqueous interface, wherein hard and/or multiply charged ions are excluded from the interface but large polarizable anions show interfacial enhancement relative to the bulk. The observed trend in the propensity of anions to adsorb at the air/water interface appears to follow an inverse order of the Hofmeister series for anions. This study focuses on experimental and theoretical examination of the partitioning behavior of perchlorate (ClO_4^-) and chloride (Cl^-) ions at the air/water interface. We have used ambient pressure X-ray photoelectron spectroscopy to directly probe the interfacial concentrations of ClO_4^- and Cl^- ions in sodium perchlorate and sodium chloride solutions, respectively. In the case of ClO_4^- ion, experimental observations are compared with molecular dynamics simulations utilizing both first principles based interaction potentials as well as polarizable classical force fields. Both the experimental and the theoretical results show enhancement of ClO_4^- ion at the interface, compared with the absence of such enhancement in the case of the Cl^- ion. Our observations are in agreement with the expected trend in the interfacial propensity of anions based on the Hofmeister series.

Introduction

There is a steadily growing body of research suggesting that the propensity of anions to adsorb at the air/water interface follows an inverse order of the Hofmeister series for anions: $SO_4^{2-} > F^- > HPO_4^{2-} > CH_3COO^- > Cl^- > Br^- > NO_3^- > ClO_3^- > I^- > ClO_4^- > SCN^-$.[1] Both recent theoretical and experimental work points toward a model wherein hard and/or multiply charged ions are excluded from the air/water interface, while large polarizable anions show enhanced presence at the interface relative to the bulk.[2−11] The propensity of large, polarizable ions for aqueous interfaces is contrary to the traditional view of an ion-free interface[12,13] and as such has garnered considerable research interest. The presence of ions at aqueous interfaces has important consequences for heterogeneous physics and chemistry relevant to both technology and environmental processes. For instance, atmospheric chemistry of aqueous sea salt aerosol is now known to be strongly influenced by the presence of halide ions at the air/water interface.[8,14]

The present study examines the propensity of perchlorate (ClO_4^-) and chloride (Cl^-) ions for the air/water interface. On the basis of its relative position within the Hofmeister series, ClO_4^- is expected to show enhanced presence at the air/water interface. The presence of ClO_4^- ions near the aqueous interface had been proposed as early as 1957 based on the measurement of negative surface potential in aqueous alkali metal perchlorate solutions.[15] Angle-resolved photoemission study by Moberg et al. also reported appreciable surface enhancement of the ClO_4^- ion in an equimolar solution of tetrabutylammonium perchlorate and potassium chloride in formamide.[16] In recent years, similar enhancement of ClO_4^- at the solution interface has been proposed, based on mass spectrometry, vibrational sum frequency spectroscopy, and surface potential measurements as well.[17,18] In contrast, molecular dynamics (MD) simulations of alkali halide solutions have proposed that the Cl^- ion is neutral with respect to its propensity for the interface; i.e., it is neither enhanced nor depleted at the interface relative to the bulk solution.[19]

Aside from its proposed interfacial behavior in aqueous solutions, ClO_4^- is also a known natural and anthropogenic contaminant with the potential to cause hypothyroidism in humans.[20] In recent years, it has attracted attention as an emerging environmental pollutant responsible for the widespread contamination of groundwater, particularly in the southwestern United States.[21−23] Physical and chemical characteristics of ClO_4^-, such as its extreme solubility and nonreactivity (due to large activation energies), make it a difficult ion to uniquely analyze for and remediate.[21] As a result, there is considerable interest in devising new technologies for the effective treatment of ClO_4^- contamination in water. In this context, detailed knowledge of the behavior of ClO_4^- ions in aqueous solutions is essential for the development of a potentially viable remediation technology, such as the selective extraction of contaminants naturally enriched at the air/water interface.

In recent years, the application of various surface sensitive experimental techniques has yielded a wealth of information regarding the nature and interaction of ions at aqueous interfaces.[2,6,9] Previous *in situ* observations have shown the interfacial enhancement of larger, more polarizable halide ions, i.e., Br^- and I^-, in aqueous salt solutions based on ambient pressure X-ray photoelectron spectroscopy (AP-XPS) measurements.[2,24] AP-XPS combines the surface sensitivity of conventional XPS analysis with the ability to acquire photoemission spectra in gaseous environments at pressures of up to several Torr.[25] This makes it a particularly suitable technique for probing

* Corresponding authors. E-mail: kuo2@llnl.gov (I-F.W.K.); sghosal@cdph.ca.gov (S.G.).
[†] Ruhr-Universität Bochum.
[‡] Physical and Life Sciences Directorate, Lawrence Livermore National Laboratory.
[§] Chemical Sciences Division, Lawrence Berkeley National Laboratory.
[∥] Present address: California Department of Public Health, Richmond, CA 94804.

10.1021/jp9053154 CCC: $40.75 © 2009 American Chemical Society
Published on Web 11/06/2009

the ion distribution near the surface region of aqueous solutions in equilibrium with their vapor. In this study, we have used AP-XPS to directly probe the concentrations of ClO_4^- and Cl^- ions at the air/water interface of aqueous sodium perchlorate ($NaClO_4$) and sodium chloride (NaCl) solutions. Our results show enhancement of the ClO_4^- ion at the air/solution interface and the absence of such an enhancement in the case of the Cl^- ion. The experimental observations of the ClO_4^- ion in solution are compared with molecular dynamics (MD) simulations of an aqueous perchlorate solution, utilizing both first principle based interaction potentials as well as polarizable classical force fields. The simulation results confirm the experimentally observed enhancement of ClO_4^- ions at the solution interface. Our observations are in agreement with the expected trend in terms of the interfacial propensity of anions based on the Hofmeister series.

Experimental Details

Ambient Pressure XPS. The AP-XPS system has been described in detail elsewhere,[25,26] and only a brief description of the features pertinent to our experiment is given here. The AP-XPS system is equipped with a differentially pumped electrostatic transfer lens system which enables the acquisition of photoemission spectra at pressures up to several Torr. This feature is critical for making *in situ* measurements on aqueous solutions in equilibrium with water vapor. In the current experiments, a saturated aqueous salt solution was generated *in situ*, starting with the dry crystalline salt and progressively increasing the relative humidity (RH) in the chamber until the formation of a solution phase was visually observed and subsequently confirmed by the presence of the condensed phase peak in the O (1s) spectrum. The requisite RH conditions for the dissolution of $NaClO_4$ and NaCl were achieved by lowering the sample temperature while maintaining a given water vapor pressure in the chamber. The sample temperature (read by a thermocouple attached to the cooling stage of the sample holder) and the water vapor pressure (read by a capacitance pressure gauge) were carefully controlled throughout the experiment to ensure continued presence of the solution phase. In the case of $NaClO_4$, water vapor pressure and sample temperature corresponding to deliquescence were ~1.7 Torr and ~ −7 °C, respectively (~60% RH). The corresponding values for NaCl deliquescence were ~1.6 Torr and ~ −10 °C (~76% RH).

In XPS, the probing depth into the sample is determined by the inelastic mean free path (IMFP) of the ejected photoelectrons, which is a function of the photoelectron kinetic energy (KE). KE in turn is determined by the incident photon energy. In these experiments, depth dependent density profiles of ions in solution were measured by varying the kinetic energy of the photoelectrons from 200−600 eV. The IMFP of photoelectrons in liquids is not well understood, and accurate estimates remain difficult to obtain.[27] However, based on the properties of neat water, we estimated that for the lowest KE (200 eV) the IMFP is equivalent to the outermost 5−11 Å, whereas at the highest KE (600 eV) it is equal to the outermost 20−30 Å of solution.[28] For the direct comparison of elemental compositions corresponding to a single probe depth, spectra of all of the elements were acquired consecutively with the same KE value at the same sample location. This methodology has been used previously to examine the preferential enhancement of the larger halide ions (Br^-, I^-) at the air/solution interface.[2,24]

First Principles Molecular Dynamics Simulations. Potential of mean force (PMF) calculation for the transport of the ClO_4^- ion across the liquid/vapor interface was carried out by constraining the ClO_4^- ion to different interfacial depths within a simulated water slab to model ion transport across the interface. The water slab consisted of 216 water molecules residing within a simulation cell of 15 Å × 15 Å × 71.44 Å. More details regarding the simulation protocols for aqueous interfacial calculations can be found elsewhere.[29,30] The PMF calculation was constructed from 26 independent first principles molecular dynamics simulations (FPMD), wherein the ion was constrained at a series of intervals, 1.06 Å apart, as a function of interfacial depth. Each independent FPMD simulation was run for a total of 5−10 ps during which the relative position of the ClO_4^- ion as a function of interfacial depth was maintained. Block averages of the average force were monitored to ensure convergence during the short sampling time allotted by FPMD. In addition, a ClO_4^- ion solvated by 64 water molecules was also simulated with 3-D periodic boundary conditions in the isobaric−isothermal ensemble (NpT) to mimic the bulk solvation environment. The condensed phase simulation was run for a total of 11 ps.

FPMD simulations were performed using the Kohn−Sham formulation of density functional theory as implemented in the QuickStep module of CP2K.[31,32] The FPMD simulations use a dual basis set method whereby the valence states are described using both Gaussian type orbitals (TZV2P) as well as a plane-wave basis set expanded up to a 280 Ry cutoff for the density.[33] The core electronic states are represented by Goedecker−Teter−Hutter type pseudopotentials.[34] In addition, Becke and Lee−Yang−Parr exchange and correlation energy functionals are utilized.[35,36] This combination has been shown to be both computationally cost-effective as well as accurate in reproducing different results from plane-wave basis calculations for aqueous solutions.[37] Efficient iterative solver as well as wave function extrapolation methods were utilized to reduce the average number of iterations required during the self-consistent field (SCF) cycle for each molecular dynamics step.[38]

Molecular Dynamics Simulations. In addition to FPMD simulations, molecular dynamics (MD) simulations utilizing polarizable force fields were performed on a 1 M $NaClO_4$ solution following the approach of Jungwirth and Tobias.[39] The three-site water model of Caldwell and Kollman, which includes polarization effects, was utilized.[40] For ClO_4^-, gas phase calculations utilizing B3LYP and MP2 with the aug-cc-pvtz basis set were performed with Gaussian 98.[41−43] The polarizabilities and hyperpolarizabilites were computed using static frequencies, while the charges were obtained using the ESP charge method.[44,45] The atomic polarizability α ($\alpha_{Cl} = 0.2$ Å^3, $\alpha_O = 0.4$ Å^3) and charge q ($q_{Cl} = 1.2$ e, $q_O = -0.55$ e) for ClO_4^- were determined from the gas phase calculations.[43] To estimate the reduction in the isotropic gas phase polarizability upon solvation, for 30 configurations from the FPMD simulation, the polarizability was calculated at the MP2 level for the bare ClO_4^- and the ion including the first solvation shell. The shell was modeled as a point charge field, where the water molecules were chosen in such a way that the Cl−O(water) distance is less than 4.25 Å. Charges of −0.8476 and 0.4238 e were assigned to the positions of the oxygens and hydrogens, respectively. The reduction of the isotropic gas phase polarizability of 1.99 Å upon solvation is about 10%. Intramolecular parameters ($r_{ClO} = 1.495$ Å, $k_{bond} = 360$ kcal·mol^{-1}·Å^{-2}; $\theta_{OClO} = 109.5°$, $k_{bend} = 140$ kcal·mol^{-1}·rad^{-2}) were fitted to match the power spectra obtained from the condensed phase FPMD simulation of ClO_4^- in the isothermal−isobaric ensemble. All Lennard-Jones (LJ) interactions between ClO_4^- and water (i.e., chlorine−hydrogen(water), chlorine−oxygen(water), and

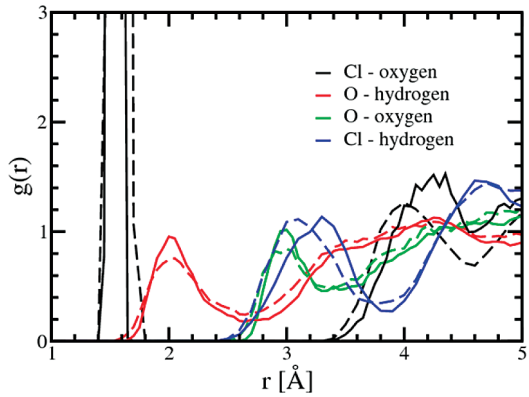

Figure 1. Pair distribution function for bulk solvated ClO_4^-. Results obtained from the first principles based interaction potential are shown as dashed lines, while polarizable force field results are shown as solid lines.

oxygen−hydrogen(water)) were explicitly set to zero with the exception of the oxygen(ClO_4^-)−oxygen(water) interaction. The oxygen(ClO_4^-) LJ interaction parameters ($\sigma = 3.3854$ Å; $\varepsilon = 0.154$ kcal/mol) were obtained by fitting to the oxygen(ClO_4^-)−oxygen(water) radial distribution function of the condensed phase FPMD simulation.

To validate the newly parametrized polarizable model for the ClO_4^- ion, bulk phase classical MD simulation for ClO_4^- using the Amber7 program in the NpT ensemble at 400 K and 1 atm was performed. The temperature and pressure were controlled using the Berendsen coupling scheme with time constants of $\tau_p = 0.1$ ps and $\tau_T = 0.2$ ps. Intermolecular interactions were cut off at 9 Å, with long-range electrostatic interactions computed via the particle-mesh Ewald method (PME).[46] The induced polarization was iteratively converged at each step to 10^{-5} D. The newly parametrized polarizable model for the ClO_4^- ion was able to reproduce the condensed phase structure of the ClO_4^- ion in the bulk when compared to the condensed phase FPMD simulation (Figure 1).

For the interfacial calculation utilizing a polarizable force field, one long simulation using the same simulation protocol was employed as described above. This interfacial system consisted of 16 Na^+, 16 ClO_4^-, and 1054 water molecules (~1 M) and was equilibrated within the isothermal−isobaric ensemble at 400 K and 1 atm using periodic boundary conditions. After 1 ns, the box was extended in the z direction (25 Å × 25 Å × 80 Å), with the water lamella placed in the center. The interface was simulated for 6 ns using a time step of 1 fs. In addition, to facilitate direct comparison to FPMD simulations, a series of 32 independent simulations was also performed for a single ClO_4^- ion with 216 water molecules, restrained at different interfacial depths within a neat air/water interface. The restraint potential was harmonic [$V(r) = 0.5 \cdot k \cdot (r - r_o)^2$] with a force constant of 44.8168 kcal·mol^{-1}·Å^{-2}.

Results and Discussion

Sodium Perchlorate ($NaClO_4$). ***Photoinduced Decomposition of $NaClO_4$.*** Figure 2 shows a series of photoemission spectra of the Cl(2p) region acquired sequentially at the same location on a dry $NaClO_4$ crystallite. The incident photon energy of 500 eV corresponds to a KE of 300 eV. From measurements of the photon flux using a calibrated photodiode, we estimate the flux density to be 5×10^{12} photons × s^{-1} × cm^{-2}. The spectra shown in Figure 2 have been charge referenced to the Na(2s) binding energy (BE) of 64.20 eV.[47] Increasing exposure

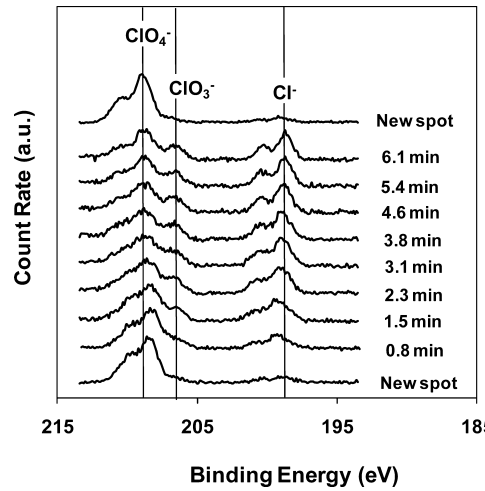

Figure 2. Ambient pressure XP spectra of the Cl(2p) region acquired sequentially at the same location on a $NaClO_4$ crystallite at a sample temperature of 21 °C and water vapor pressure of 1.6 Torr, which corresponds to ~5% relative humidity condition. The incident photon energy is 500 eV which corresponds to a KE of 300 eV. The spectra have been charge referenced to the Na(2s) orbital set at 64.20 eV, characteristic of solid $NaClO_4$.

to the incident X-rays alters the chemistry of the Cl containing species. This is evidenced by the appearance of additional spectral features, corresponding to chlorate (ClO_3^-) and chloride (Cl^-) species, along with ClO_4^-, with continued X-ray exposure. Peak intensities associated with the various species (ClO_4^-, ClO_3^-, Cl^-) are dependent on the X-ray exposure time; i.e., the ClO_4^- peak intensity decreases with increasing exposure, while the ClO_3^- and Cl^- peaks grow in intensity over time. However, spectra acquired at previously unexamined (new) locations on the sample are dominated by the ClO_4^- peak and show minimal presence of ClO_3^- and Cl^- species. The observed behavior is attributed to the photoinduced decomposition of ClO_4^- ions into ClO_3^- and Cl^- species, a phenomenon that was reported previously by Copperwaite et al.[48] On the basis of their observations, Copperwaite et al. concluded that the "photoinduced decomposition of ClO_4^- proceeds via simple consecutive first-order processes involving ClO_3^- as an intermediate." In the case of NaCl, we have previously observed similar photoinduced loss of Cl^- species as a function of X-ray exposure. In contrast to ClO_4^- and Cl^-, the influence of photoinduced decomposition on Na^+ is negligible over the time scale of our experiment.

Figure 3 shows a plot of the relative concentrations of ClO_4^-, ClO_3^-, and Cl^- species as a function of the X-ray exposure time. Relative concentrations of the individual species are expressed as fractions of the total integrated XP spectral areas corresponding to all three species. Fitting of the relative ClO_4^- concentration as a function of X-ray exposure time in Figure 3 gives a time constant of 1.6 min for the photoinduced decomposition process. In subsequent measurements to determine the depth resolved distribution of the ClO_4^- ion in the solution, several precautionary measures were taken to minimize the influence of photoinduced decomposition on the results. For instance, each new set of spectra (Cl2p, Na2s, and O1s) for a given KE was always acquired at a fresh spot on the sample. Also, the Cl(2p) spectrum was always acquired first, and the acquisition time was limited to less than a minute.

Depth Resolved Distribution of ClO_4^- Ion in an Aqueous $NaClO_4$, Solution. To examine the propensity of ClO_4^- ions for the solution/vapor interface, we used AP-XPS to measure

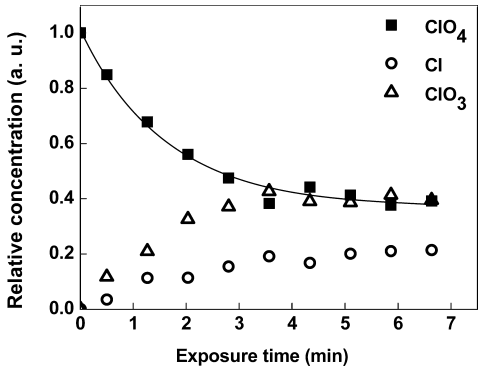

Figure 3. Relative concentrations of ClO_4^-, ClO_3^-, and Cl^- species measured in a dry $NaClO_4$ crystallite as a function of X-ray exposure to an incident photon energy of 500 eV which corresponds to a KE of 300 eV. The trend line through ClO_4^- data points represents a fit to a first order rate equation.

the depth resolved distribution of the ions in aqueous $NaClO_4$ solution. Relative concentrations of the various ions as a function of depth into the solution were determined using XP spectra corresponding to the Na(2s), Cl(2p), and O(1s) regions, acquired for KEs of 200, 300, 400, and 600 eV. Figure 4 presents XP spectra corresponding to the O(1s), Cl(2p), and Na(2s) core levels acquired at 200 eV KE in a saturated $NaClO_4$ solution which formed at a sample temperature of −7 °C and a water vapor pressure of 1.7 Torr. The depth-dependent distributions of ClO_4^- ions in the solution are expressed as ClO_4^-/Na^+ and ClO_4^-/O ratios (Figure 5). The ratios ClO_4^-(Cl2p)/Na^+(Na2s) and ClO_4^-(Cl2p)/O(O1s), determined from the corresponding integrated XP spectral areas, were normalized using the approach outlined below. In the case of dry $NaClO_4$, the expected values (in the absence of photoinduced decomposition) for the ClO_4^-/Na^+ and ClO_4^-/O ratios are 1 and 0.25, respectively, independent of the probe depth. On the basis of this information, sensitivity factors for the normalization of ClO_4^-/Na^+ and ClO_4^-/O ratios measured in the aqueous $NaClO_4$ solution were determined using the expected values of dry ratios and the experimentally measured Cl(2p), Na(2s), and O(1s) XP spectral areas corresponding to dry (∼10% relative humidity) $NaClO_4$ crystallites. The normalized ClO_4^-/O ratio in the aqueous solution (obtained using the O(1s) peak area associated with condensed phase liquid water) as a function of KE is a measure of the depth dependent ClO_4^- concentration in the solution. However, we would like to note that the O(1s) peak for the condensed phase water (535 eV BE) overlaps with the O(1s) peak associated with the ClO_4^- ion (533 eV BE). As a result, the experimentally measured O(1s) peak area for water in the saturated solution is expected to include a finite contribution from the ClO_4^- related O(1s) species, thereby potentially resulting in overestimation of the condensed water peak area. The molecular ratio of ClO_4^-/H_2O in the bulk for a saturated solution is 0.06; i.e., the ratio of $O(ClO_4^-)/O(H_2O)$ is 0.24.[49] We therefore estimate that the amount of water, measured from the O1s signal, is overestimated by less than 25%. The actual error is expected to be considerably smaller due to the beam-induced reduction of the ClO_4^- species. While precautions were taken to minimize the photoinduced decomposition of ClO_4^- during measurement, nevertheless, the Cl(2p) spectral region showed small but finite contributions from the decomposition products, namely, ClO_3^- and Cl^-. The ClO_4^- results shown in Figures 5 and 6 were calculated using only the Cl(2p) peak area associated with the ClO_4^- species. Therefore, it is likely that the actual ClO_4^- concentration in the solution is larger than our calculated value. This is true for all of the experimental probe depths and as such does not influence the depth dependent comparison of ClO_4^- concentration in the solution. The experimentally measured depth dependent distributions of ClO_4^- ions in the solution are shown in Figure 5 where we have plotted the ClO_4^-/Na^+ ratio as well as the concentration of ClO_4^- as a function of KE. Both the ClO_4^-/Na^+ ratio and the concentration of ClO_4^- in the solution decrease with increasing KE, with the highest concentration corresponding to the lowest KE, and hence most representative of the interfacial region. The observed trend is indicative of the enhancement of ClO_4^- ion at the interface relative to the bulk solution as well as the cation (Na^+).

A slight depression in the ClO_4^-/Na^+ ratio is observed in Figure 5, corresponding to a KE of 400 eV. MD simulations predict the formation of a double layer with respect to anion versus cation distributions near the solution/vapor interface (see Figure 8). Na^+ ions are expected to remain well solvated in the interior of the solution, while ClO_4^- ions occupy a significant fraction of the interface. Therefore, it is possible that the depression in the ClO_4^-/Na^+ ratio just below the interface is indicative of the proposed double layer formation. However, we would like to note that we cannot make a definitive statement about the formation of the double layer based on our data alone, since the small depression in the ClO_4^-/Na^+ ratio is within the margins of our experimental error.

Figure 6 shows a direct comparison of the experimentally measured concentrations of ClO_4^- and Na^+ ions in the AP-XPS experiment (expressed as ClO_4^-/O and Na^+/O ratios, respectively) with the concentrations expected based on bulk thermodynamic data for a saturated $NaClO_4$ solution in the absence of interfacial enhancement of ClO_4^-.[49] The expected concentrations of the ions in a bulk saturated solution (3.5 M) were determined based on salt solubility data at the relevant temperature (−6.8 °C).[49] The experimentally measured concentration of ClO_4^- ion at the solution/vapor interface (200 eV KE) is significantly greater than the value expected for a bulk saturated $NaClO_4$ solution. However, the ClO_4^- concentration measured at a larger depth into the solution (600 eV KE) is in excellent agreement with the value expected for a saturated solution. Therefore, our results show that in aqueous $NaClO_4$ solution the concentration of ClO_4^- ions at the interface is significantly greater than the expected as well as the measured bulk concentration of ClO_4^-.

Comparison of Experiment with Simulation Results. The enhancement of ClO_4^- ion at the liquid/vapor interface is supported by results from FPMD simulations. Preferential solvation sites for the ClO_4^- ion in a water slab can be deduced from Figure 7 which shows the average constraint force in the z direction, $\langle F_{const} \rangle$, exerted on ClO_4^- as a function of depth. A value of $\langle F_{const} \rangle$ close to zero indicates that there is minimal force acting on the ion in the z direction and hence the corresponding depth represents a stable solvation site or local minimum. On the basis of the values of $\langle F_{const} \rangle$ plotted in Figure 7B, the ClO_4^- ion in the simulation has two stable solvation sites located (1) at the center of the slab (∼ −15 Å) and (2) near the Gibbs dividing surface (GDS) (0.0 Å). However, the potential of mean force computed via $\langle F_{const} \rangle$ indicates a stabilization of ClO_4^- at the interface by ∼16 kcal/mol, which does not take into account the slow fluctuations (i.e., expansion or contraction) of the interface on the picosecond time scale. Thus, the average force on ClO_4^- in the z direction can be approximated as $\langle F_z \rangle = \langle F_{const} \rangle - \langle F_{fluct} \rangle$, where $\langle F_{const} \rangle$ is the constraint force shown in Figure 7B and $\langle F_{fluct} \rangle$ is the contribution from fluctuations of the whole interface. To estimate $\langle F_{fluct} \rangle$,

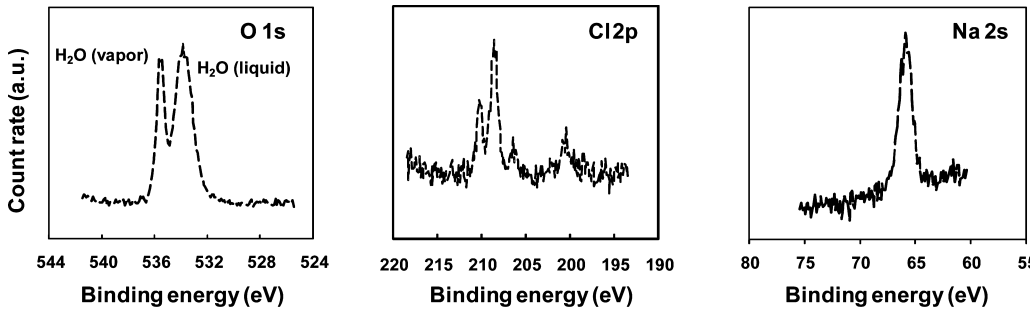

Figure 4. AP-XP spectra of the O(1s), Cl(2p), and Na(2s) core levels in a saturated $NaClO_4$ solution acquired at 200 eV photoelectron kinetic energy.

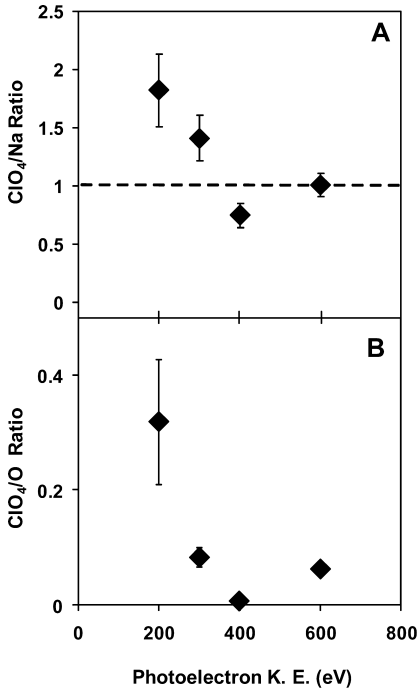

Figure 5. Integrated XP peak area ratios, (A) ClO_4^-(Cl2p)/Na^+(Na2s) and (B) ClO_4^-(Cl2p)/O(O1s) ($H_2O_{(l)}$), as a function of photoelectron kinetic energy for a saturated $NaClO_4$ aqueous solution. The average value of multiple measurements is shown, with the error bar representing the standard error in the measurement. Each data point was collected on a fresh sample spot as a means to minimize the loss of halogen signal due to X-ray beam damage. The dashed line in part A represents the expected bulk ratio in the absence of segregation.

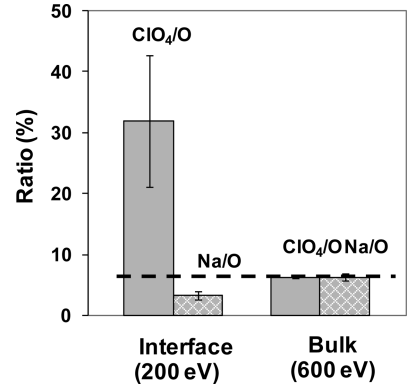

Figure 6. Experimentally measured concentrations of ions (expressed as integrated XP peak area ratios) in a saturated $NaClO_4$ solution for two different photoelectron kinetic energies: 200 eV (interface) and 600 eV (bulk). Error bars indicating standard error are shown for the experimental measurements. The dashed line indicates the ionic concentration derived from literature based thermodynamic data for a bulk, saturated $NaClO_4$ solution.

assumptions can be made that $\langle F_z \rangle$ for ClO_4^- in the bulk region should be zero, and $\langle F_{\text{fluct}} \rangle$ is the same in the bulk and at the interface. The PMFs obtained from thermodynamic integration of $\langle F_{\text{const}} \rangle$ and the newly derived $\langle F_z \rangle$ are shown in Figure 7C. This analysis reveals that fluctuations of the whole water slab can have a significant effect on the computed PMF when the sampling time is on the same time scale. The ClO_4^- is predicted to have a stabilization energy of around ~3 kcal/mol at the interface over the bulk. Finally, the FPMD simulations were monoionic, consisting of a single ClO_4^- ion in the water slab, and therefore, screening or high ionic concentration effects were ignored.

In addition to the FPMD simulations, polarizable force field based MD simulations also show a large surface enhancement of ClO_4^- ion relative to both the cation and the bulk solution (Figure 8). Simulation of a 1 M $NaClO_4$ slab shows the formation of a double layer with respect to the anion and cation distribution near the interface with a maximum ClO_4^- density at approximately −0.5 Å, equating to a relative enhancement of ~9 when compared to the bulk ClO_4^- density. Using the probability distribution, $P(z)$, the free energy, $G(z)$, can be evaluated as $G(z) = -k_B T \ln(P(z)/P^0(z))$, where $P^0(z)$ is chosen such that the global minimum is equal zero. This can be directly compared to equivalent PMF results from FPMD and the PMF from umbrella sampling with polarizable force fields.[50] The PMF and stabilization energies for all three sets of calculations are shown in Figure 9. All three theoretical approaches indicate a stabilization energy for ClO_4^- around 1.5−3 kcal/mol, with the lowest and highest value obtained from the monoionic interface using a polarizable force field and DFT interaction potential, respectively. Additionally, the energetic barrier between the interface and bulk regions increased by ~1 kcal/mol with the presence of additional ions, possibly due to ion layering. This indicates a large concentration dependence for the diffusion rate of ClO_4^- in the z direction. Although both FPMD and polarizable force field based MD simulations predict surface enhancement of ClO_4^-, it is interesting to note that FPMD predicts that ClO_4^- ion is situated slightly above the GDS, whereas the polarizable force field predicts maximum enhancement slightly below the GDS. This disparity could be due to the limitation of the polarizable force field to describe partial solvation as would occur above the GDS. Overall, both simulation methods are in good agreement with the AP-XPS based experimental results wherein the surface enhancement of ClO_4^- ions in solution was measured directly.

Figure 10 shows a quantitative comparison between the AP-XPS experiment and the polarizable force field based MD simulation results. For the purpose of comparison, the theoretical

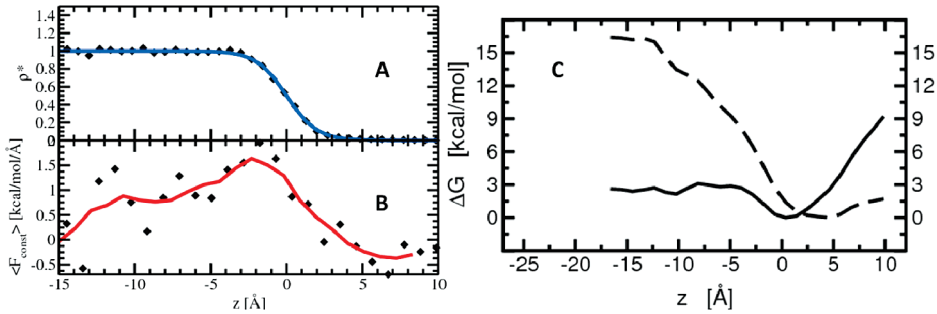

Figure 7. (A) Density profile of water from first principles molecular dynamics (filled diamonds), fitted to $\rho(z) = 0.5\rho_l[1 - \tanh((z - z_{GDS})/\delta)]$ (blue line). The density profile was normalized to the fitted bulk density of the slab of 0.845 g/cm^3. The Gibbs dividing surface was obtained from the density profile and set to 0.0 Å in the current figure. (B) The average constraint force profile (filled diamonds) for the ClO_4^- ion in the z direction. The red line represents the running average computed over three nearest data points. (C) Potential of mean force computed from the average constraint force (dashed line), $\langle F_{const}\rangle$, and the average force in the z direction (solid line), $\langle F_z\rangle$, once fluctuations are accounted for.

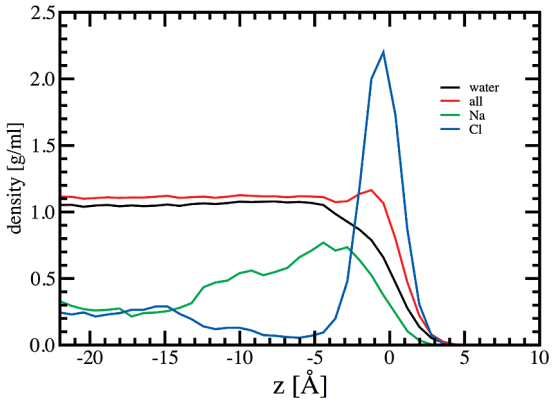

Figure 8. Density profiles obtained from polarizable force field molecular dynamics simulation of a water slab containing 16 Na^+, 16 ClO_4^-, and 1054 water molecules. The Gibbs dividing surface is set to 0.0 Å.

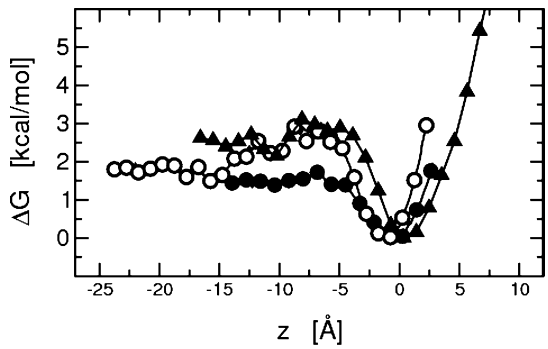

Figure 9. Free-energy profiles obtained for ClO_4^- anion using (1) thermodynamic integration with a DFT interaction potential (solid triangles), (2) umbrella sampling with a polarizable force field (solid circles), and (3) ~1 M solution (16 $NaClO_4$ and 1054 water molecules) inverting the anion distribution from a simulation utilizing a polarizable force field (open circles).

ion densities as predicted by the MD simulation were converted into simulated XPS ionic ratios using the convolution integral

$$\int e^{(-Z/\Gamma(KE))}\rho(z)\,dz$$

where z is the distance into the solution from the solution/vapor interface, $\rho(z)$ is the ion density as a function of depth into the solution, obtained from the results of the MD simulations, and Γ(KE) is the IMFP of the photoelectrons which is a function of the KE. Both AP-XPS experiment and the converted simulation results show a decrease in the ClO_4^-/Na^+ ratio with increasing

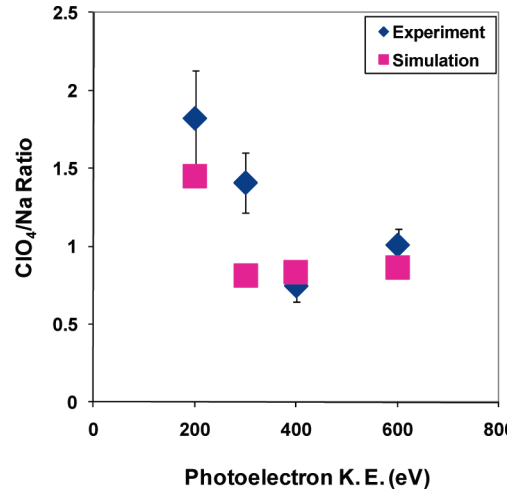

Figure 10. Measured and predicted ClO_4^-/Na^+ atomic ratios in aqueous solutions of $NaClO_4$ as a function of photoelectron kinetic energy. The blue diamonds are the experimental results corresponding to the saturated $NaClO_4$ solution, while the magenta squares are the atomic ratio calculated from the MD simulation of a 1 M $NaClO_4$ solution. The predicted atomic ratio is calculated by integration of a convolution integral for each ion.

KE, thereby indicating preferential enhancement of ClO_4^- at the interface relative to the bulk. While both theory and experiment show a similar trend in the ClO_4^-/Na^+ ratio as a function of KE, the actual numbers differ in their magnitude. The observed discrepancy between experimentally measured and theoretically predicted ion ratios may be a result of the difference in solution concentrations probed in the experiment versus the MD simulation, i.e., saturated versus unsaturated solution, respectively. Also, the dependence of IMFP on KE may be different from our present estimate, which in turn would influence the predicted ratios.

Sodium Chloride (NaCl). ***Depth Resolved Distribution of Cl^- Ion in an Aqueous NaCl Solution.*** In the past decade, MD simulations of aqueous interfaces have proposed that Cl^- ions in solution are neither strongly repelled nor enhanced at the solution/vapor interface.[19] We have used AP-XPS based measurements to verify the proposed distribution profile of Cl^- ions in aqueous NaCl solution. Quantification of the experimentally measured Cl^- distribution in the solution was accomplished using a normalization procedure similar to the one described above for $NaClO_4$. Sensitivity factors for the normalization of Cl(2p)/Na(2s) ionic ratios measured in the solution at each KE were determined based on measurements on the dry salt (5% RH), wherein the Cl^-/Na^+ ratio is expected to be 1, independent

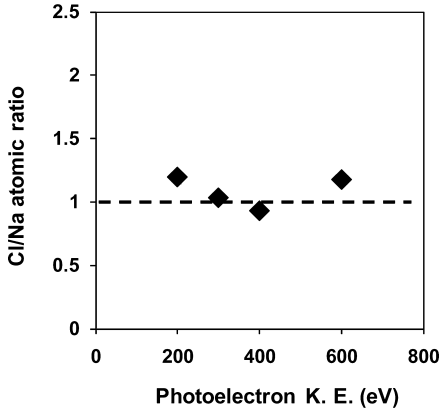

Figure 11. Integrated XP peak area ratio, Cl^-(Cl2p)/Na^+(Na2s), as a function of photoelectron kinetics for a saturated NaCl aqueous solution. The average value of multiple measurements is shown, with the error bar representing the standard error in the measurement. Each data point was collected on a fresh sample spot as a means to minimize the loss of halogen signal due to X-ray beam damage. The dashed line represents the expected bulk ratio in the absence of segregation.

of KE. The normalized Cl^-/Na^+ ratios for the deliquesced salt as a function of KE are shown in Figure 11. The measured Cl^-/Na^+ ratios as a function of increasing KE, hence increasing depth into the solution, do not show any evidence of Cl^- ion enhancement at the interface. The ratios are clustered around the value of 1, independent of probe depth. Therefore, the measured depth dependent distribution of Cl^- ions in an aqueous NaCl solution appears to be in qualitative agreement with the predictions of MD simulation.[11] Similar absence of the interfacial enhancement of Cl^- ions in solution has been observed previously in a study involving a mixed aqueous solution of NaCl and NaBr.[24]

Conclusion

We have used ambient pressure X-ray photoelectron spectroscopy to examine the ion density profiles of ClO_4^- and Cl^- ions in aqueous solutions of their respective sodium salts. Our results show that ClO_4^- ions are enriched at the solution/vapor interface relative to the bulk. The AP-XPS experimental observations are supported by FPMD and MD simulations of the solution/vapor interface of aqueous $NaClO_4$ solution. The interfacial behavior of ClO_4^- ions in solution is in contrast to that of Cl^- ions which are shown to be neutral with respect to interfacial enhancement. These observations support a growing body of research suggesting that the propensity of various anions toward the solution/vapor interface follows an inverse order of the Hofmeister series. Partitioning behavior of Cl^- ions in solution has previously been examined by MD simulations as well as experimental measurements.[4,6,9,51] The depth dependent distribution of Cl^- ion reported here is in agreement with these previous studies. For both Cl^- and ClO_4^- ions, the effect of photoinduced decomposition is an important consideration in using X-ray based analytical techniques such as AP-XPS.

Acknowledgment. The ALS and the Molecular Environmental Science beamline (11.0.2) are supported by the Director, Office of Science, Office of Basic Energy Sciences, Division of Chemical Sciences, Geosciences, and Biosciences and Materials Sciences Divisions of the U.S. Department of Energy at the LBNL under contract DE-AC02-05CH11231. Computing resources were provided by Livermore Computing. We would like to thank LLNL Computing staff for their help. We would also like to thank William Boucier for helpful discussions regarding the relevance of this work in terms of potential water treatment technology. This work was performed under the auspices of the U.S. Department of Energy by Lawrence Livermore National Laboratory under contract DE-AC52-07NA27344.

Note Added in Proof. Following the submission of this manuscript we were made aware of another study probing the distribution of ClO_4^- ions in aqueous solution.[52] Their observations are in agreement with our results.

References and Notes

(1) Hofmeister, F. *Naunyn-Schmiedeberg's Arch. Exp. Pathol. Pharmakol. (Leipzig)* **1888**, *24*, 247–260.
(2) Ghosal, S.; Hemminger, J. C.; Bluhm, H.; Mun, B. S.; Hebenstreit, E. L. D.; Kettler, G.; Ogletree, D. F.; Requejo, F. G.; Salmeron, M. *Science* **2005**, *307*, 563–566.
(3) Jungwirth, P.; Tobias, D. J. *Chem. Rev.* **2006**, *106*, 1259–1281.
(4) Chang, T. M.; Dang, L. X. *Chem. Rev.* **2006**, *106*, 1212–1233.
(5) Jungwirth, P.; Winter, B. *Annu. Rev. Phys. Chem.* **2008**, *59*, 343–366.
(6) Gopalakrishnan, S.; Liu, D. F.; Allen, H. C.; Kuo, M.; Shultz, M. J. *Chem. Rev.* **2006**, *106*, 1155–75.
(7) Jungwirth, P.; Finlayson-Pitts, B. J.; Tobias, D. J. *Chem. Rev.* **2006**, *106*, 1137–39.
(8) Knipping, E. M.; Lakin, M. J.; Foster, K. L.; Jungwirth, P.; Tobias, D. J.; Gerber, R. B.; Dabdub, D.; Finlayson-Pitts, B. J. *Science* **2000**, *288*, 301–306.
(9) Petersen, P. B.; Saykally, R. J. *Chem. Phys. Lett.* **2004**, *397*, 51–55.
(10) Petersen, P. B.; Saykally, R. J. *Annu. Rev. Phys. Chem.* **2006**, *57*, 333–64.
(11) Jungwirth, P.; Tobias, D. J. *J. Phys. Chem. B* **2002**, *106*, 6361–6373.
(12) Onsager, L.; Samaras, N. N. T. *J. Chem. Phys.* **1934**, *2*, 528–36.
(13) Adam, N. K. *The Physics and Chemistry of Surfaces*; Oxford University Press: London, 1941.
(14) Hunt, S. W.; Roeselová, M.; Wang, W.; Wingen, L. M.; Knipping, E. M.; Tobias, D. J.; Dabdub, D.; Finlayson-Pitts, B. J. *J. Phys. Chem. A* **2004**, *108*, 11559–11572.
(15) Randles, J. E. B. *Discuss. Faraday Soc.* **1957**, *24*, 194–99.
(16) Moberg, R.; Bokman, F.; Bohman, O.; Siegbahn, H. O. G. *J. Am. Chem. Soc.* **1991**, *113*, 3663–67.
(17) Cheng, J.; Vecitis, C. D.; Hoffmann, M. R.; Colussi, A. J. *J. Phys. Chem. B* **2006**, *110*, 25598–25602.
(18) Gurau, M. C.; Lim, S.-M.; Castellana, E. T.; Albertorio, F.; Kataoka, S.; Cremer, P. S. *J. Am. Chem. Soc.* **2004**, *126*, 10522–23.
(19) Jungwirth, P.; Tobias, D. J. *Chem. Rev.* **2006**, *106*, 1259–81.
(20) Wolff, J. *Pharmacol. Rev.* **1998**, *50*, 89–105.
(21) Urbansky, E. T. *Biorem. J.* **1998**, *2*, 81–95.
(22) Urbansky, E. T. *Environ. Sci. Pollut. Res.* **2002**, *9*, 187–92.
(23) Parker, D. R.; Seyfferth, A. L.; Reese, B. K. *Environ. Sci. Technol.* **2008**, *42*, 1465–71.
(24) Ghosal, S.; Brown, M. A.; Bluhm, H.; Krisch, M. J.; Salmeron, M.; Jungwirth, P.; Hemminger, J. C. *J. Phys. Chem. A* **2008**, *112*, 12378.
(25) Ogletree, D. F.; Bluhm, H.; Lebedev, G.; Fadley, C. S.; Hussian, Z.; Salmeron, M. *Rev. Sci. Instrum.* **2002**, *73*, 3872.
(26) Ogletree, D. F.; Bluhm, H.; Hebenstreit, E. B.; Salmeron, M. *Nucl. Instrum. Methods Phys. Res., Sect. A* **2009**, *12*, 155.
(27) Winter, B.; Faubel, M. *Chem. Rev.* **2006**, *106*, 1176–211.
(28) Powell, C. J.; Jablonski, A. NIST Electron Inelastic-Mean-Free-Path Database - Version 1.1; National Institute of Standards and Technology: Gaithersburg, MD, 2000.
(29) Kuo, I. F. W.; Mundy, C. J.; Eggimann, B. L.; McGrath, M. J.; Siepmann, J. I.; Chen, B.; Vieceli, J.; Tobias, D. J. *J. Phys. Chem. B* **2006**, *110*, 3738–3746.
(30) Brown, M. A.; D'Auria, R.; Kuo, I. F. W.; Krisch, M. J.; Starr, D. E.; Bluhm, H.; Tobias, D. J.; Hemminger, J. C. *Phys. Chem. Chem. Phys.* **2008**, *10*, 4778–4784.
(31) CP2K (http://cp2k.berlios.de).
(32) VandeVondele, J.; Krack, M.; Mohamed, F.; Parrinello, M.; Chassaing, T.; Hutter, R. *Comput. Phys. Commun.* **2005**, *167*, 103–128.
(33) Lippert, G.; Hutter, J.; Parrinello, M. *Mol. Phys.* **1997**, *92*, 477.
(34) Goedecker, S.; Teter, M.; Hutter, J. *Phys. Rev. B* **1996**, *54*, 1703.
(35) Becke, A. D. *Phys. Rev. A* **1988**, *38*, 3098.
(36) Lee, C.; Yang, W.; Parr, R. G. *Phys. Rev. B* **1988**, *37*, 785–9.

(37) Kuo, I. F. W.; Mundy, C. J.; McGrath, M. J.; Siepmann, J. I.; VandeVondele, J.; Sprik, M.; Hutter, J.; Chen, B.; Klein, M. L.; Mohamed, F.; Krack, M.; Parrinello, M. *J. Phys. Chem. B* **2004**, *108*, 12990–12998.

(38) VandeVondele, J.; Hutter, J. *J. Chem. Phys.* **2003**, *118*, 4365–4369.

(39) Jungwirth, P.; Curtis, J. E.; Tobias, D. J. *Chem. Phys. Lett.* **2003**, *367*, 704–710.

(40) Caldwell, J. W.; Kollman, P. A. *J. Phys. Chem.* **1995**, *99*, 6208–6219.

(41) Woon, D. E.; Dunning, T. H. *J. Chem. Phys.* **1993**, *98*, 1358–1371.

(42) Kendall, R. A.; Dunning, T. H.; Harrison, R. J. *J. Chem. Phys.* **1992**, *96*, 6796–6806.

(43) Frisch, M. J.; Trucks, G. W.; Schlegel, H. B.; Scuseria, G. E.; Robb, M. A.; Cheeseman, J. R.; Zakrzewski, V. G.; Montgomery, J. A., Jr.; Stratmann, R. E.; Burant, J. C.; Dapprich, S.; Millam, J. M.; Daniels, A. D.; Kudin, K. N.; Strain, M. C.; Farkas, O.; Tomasi, J.; Barone, V.; Cossi, M.; Cammi, R.; Mennucci, B.; Pomelli, C.; Adamo, C.; Clifford, S.; Ochterski, J.; Petersson, G. A.; Ayala, P. Y.; Cui, Q.; Morokuma, K.; Malick, D. K.; Rabuck, A. D.; Raghavachari, K.; Foresman, J. B.; Cioslowski, J.; Ortiz, J. V.; Stefanov, B. B.; Liu, G.; Liashenko, A.; Piskorz, P.; Komaromi, I.; Gomperts, R.; Martin, R. L.; Fox, D. J.; Keith, T.; Al-Laham, M. A.; Peng, C. Y.; Nanayakkara, A.; Gonzalez, C.; Challacombe, M.; Gill, P. M. W.; Johnson, B. G.; Chen, W.; Wong, M. W.; Andres, J. L.; Head-Gordon, M.; Replogle, E. S.; Pople, J. A. *Gaussian 98*, revision A6; Gaussian, Inc.: Pittsburgh, PA, 1998.

(44) Singh, U. C.; Kollman, P. A. *J. Comput. Chem.* **1984**, *5*, 129–145.

(45) Besler, B. H.; Merz, K. M.; Kollman, P. A. *J. Comput. Chem.* **1990**, *11*, 431–439.

(46) Toukmaji, A.; Sagui, C.; Board, J.; Darden, T. *J. Chem. Phys.* **2000**, *113*, 10913–10927.

(47) Wren, A. G.; Phillips, R. W.; Tolentino, L. U. *J. Colloid Interface Sci.* **1979**, *70*, 544–557.

(48) Copperthwaite, R. G.; Lloyd, J. *J. Chem. Soc., Dalton Trans.* **1977**, 1117–1121.

(49) *Solubilities of lnorganic and Organic Compounds*; Stephen, H., Stephen, T., Eds.; Pergamon Press: Oxford, U.K., 1963.

(50) Kumar, S.; Bouzida, D.; Swendsen, R. H.; Kollman, P. a.; Rosenberg, J. M. *J. Comput. Chem.* **1992**, *13*, 1011–1021.

(51) Jungwirth, P.; Tobias, D. J. *J. Phys. Chem. A* **2002**, *106*, 379–383.

(52) Ottosson, N.; Vacha, R.; Aziz, E. F.; Pokapanich, W.; Eberhardt, W.; Svensson, S.; Ohrwall, G.; Jungwirth, P.; Bjorneholm, O.; Winter, B. *J. Phys. Chem.*, submitted for publication, **2009**.

JP9053154